Superdiffusive Dispersals Impart the Geometry of Underlying Random Walks

V. Zaburdaev,[1,2] I. Fouxon,[3] S. Denisov,[4,5,6] and E. Barkai[3]

[1]*Max Planck Institute for the Physics of Complex Systems, Nöthnitzer Strasse 38, D-01187 Dresden, Germany*
[2]*Institute of Supercomputing Technologies, Lobachevsky State University of Nizhny Novgorod, 603140 Nizhny Novgorod, Russia*
[3]*Department of Physics, Institute of Nanotechnology and Advanced Materials, Bar-Ilan University, Ramat-Gan 52900, Israel*
[4]*Department of Applied Mathematics, Lobachevsky State University of Nizhny Novgorod, 603140 Nizhny Novgorod, Russia*
[5]*Sumy State University, Rimsky-Korsakov Street 2, 40007 Sumy, Ukraine*
[6]*Institute of Physics, University of Augsburg, Universitätsstrasse 1, D-86135 Augsburg, Germany*

It is recognized now that a variety of real-life phenomena ranging from diffusion of cold atoms to the motion of humans exhibit dispersal faster than normal diffusion. Lévy walks is a model that excelled in describing such superdiffusive behaviors albeit in one dimension. Here we show that, in contrast to standard random walks, the microscopic geometry of planar superdiffusive Lévy walks is imprinted in the asymptotic distribution of the walkers. The geometry of the underlying walk can be inferred from trajectories of the walkers by calculating the analogue of the Pearson coefficient.

Introduction.—The Lévy walk (LW) model [1–3] was developed to describe spreading phenomena that were not fitting the paradigm of Brownian diffusion [4]. Still looking like a random walk, see Fig. 1, but with a very broad distribution of the excursions' lengths, the corresponding processes exhibit dispersal faster than in the case of normal diffusion. Conventionally, this difference is quantified with the mean squared displacement (MSD), $\langle r^2(t) \rangle \propto t^\alpha$, and the regime with $\alpha > 1$ is called superdiffusion. Examples of such systems range from cold atoms moving in dissipative optical lattices [5] to T cells migrating in the brain tissue [6]. Most of the existing theoretical results, however, were derived for one-dimensional LW processes [3]. In contrast, real-life phenomena—biological motility (from bacteria [7] to humans [8] and autonomous robots [9,10]), animal foraging [11,12], and search [13]—happen in two dimensions. Somewhat surprisingly, generalizations of the Lévy walks to two dimensions are still virtually unexplored.

In this work we extend the concept of LWs to two dimensions. Our main finding is that the microscopic geometry of planar Lévy walks reveals itself in the shape of the asymptotic probability density functions (PDFs) $P(\mathbf{r}, t)$ of finding a particle at position $\mathbf{r}$ at time t after it was launched from the origin. This is in sharp contrast to the standard 2D random walks, where, by virtue of the central limit theorem [14], the asymptotic PDFs do not depend on the geometry of the walks and have a universal form of the two-dimensional Gaussian distribution [15,16].

Models.—We begin with a core of the Lévy walk concept [1,2]: A particle performs ballistic moves with constant speed, alternated by instantaneous reorientation events, and the length of the moves is a random variable with a power-law distribution. Because of the constant speed v_0, the length l_i and duration τ_i of the ith move are linearly coupled, $l_i = v_0 \tau_i$. As a result, the model can be equally

well defined by the distribution of ballistic move (flight) times:

$$\psi(\tau) = \frac{1}{\tau_0} \frac{\gamma}{(1 + \tau/\tau_0)^{1+\gamma}}, \qquad \tau_0, \gamma > 0. \qquad (1)$$

Depending on the value of γ, it can lead to a dispersal $\alpha = 1$, typical for normal diffusion ($\gamma > 2$), and very long excursions leading to the fast dispersal with $1 < \alpha \leq 2$ in the case of superdiffusion ($0 < \gamma < 2$). At each moment of time t the finite speed sets the ballistic front beyond which there are no particles. Below, we consider three intuitive models of two-dimensional superdiffusive dispersals.

(a) The simplest way to obtain a two-dimensional Lévy walk out of the one-dimensional one is to assume that the motions along each axis, x and y, are identical and independent one-dimensional LW processes, as shown in Fig 1(a). The two-dimensional PDF, $P(\mathbf{r}, t)$, $\mathbf{r}(t) = \{x(t), y(t)\}$, of this product model is given by the product of two one-dimensional LW PDFs, $P_{\text{prod}}(\mathbf{r}, t) = P_{\text{LW}}(x, t) \times P_{\text{LW}}(y, t)$. On the microscopic scale, each ballistic event corresponds to the motion along either the diagonal or antidiagonal. Every reorientation only partially erases the memory about the last ballistic flight: while the direction of the motion along one axis could be changed, the direction along the other axis almost surely remains the same. The ballistic front has the shape of a square with borders given by $|x| = |y| = v_0 t$.

(b) In the *XY* model, a particle is allowed to move only along one of the axes at a time. A particle chooses a random flight time τ from Eq. (1) and one out of four directions. Then it moves with a constant speed v_0 along the chosen direction. After the flight time has elapsed, a new random direction and a new flight time are chosen. This process is
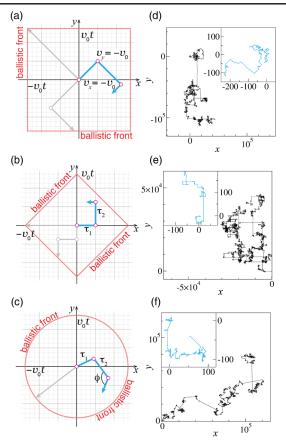
FIG. 1.   Three models of Lévy walks on a plane. (a) In the product model, x and y coordinates of a particle change according to two independent 1D Lévy walks along the coordinate axes. Whenever a direction of motion of one of the two LWs changes, there is a kink in the trajectory (∘). The ballistic front is given by $|x| = |y| = v_0 t$ (red line). (b) In the XY model, a particle is allowed to move with a speed v_0 only along one axis at a time which is chosen randomly at the reorientation points ∘. The ballistic front is specified by the condition $|x| + |y| = v_0 t$. (c) In the uniform model, at each reorientation point ∘, a particle chooses a random direction of motion, specified by an angle ϕ uniformly distributed in the interval $[0, 2\pi]$, and then moves with a constant speed v_0. The ballistic front is a circle of the radius $v_0 t$. (d–f) Trajectories produced by the models (a–c) after time $t = 10^6$. Note that on the large time scale the trajectories of the product and XY models appear to be similar. The insets show trajectories at $t = 10^3$. The parameters are $\gamma = 3/2$, $v_0 = 1$, and $\tau_0 = 1$.

sketched in Fig. 1(b). The ballistic front is a square defined by the equation $|x| + |y| = v_0 t$.

(c) The uniform model follows the original definition by Pearson [17]. A particle chooses a random direction, parametrized by the angle ϕ, uniformly distributed in the interval $[0, 2\pi]$, and then moves ballistically for a chosen flight time. The direction of the next flight is chosen randomly and independently of the direction of the elapsed flight. The corresponding trajectory is sketched

in Fig. 1(c). The ballistic front of the model is a circle $|\mathbf{r}| = v_0 t$.

Governing equations.—We now derive equations describing the density of particles for the XY and uniform models. The following two coupled equations govern the space-time evolution of the PDF [3]:

$$\nu(\mathbf{r}, t) = \int_0^t d\tau \int d\mathbf{v}\nu(\mathbf{r} - \mathbf{v}\tau, t - \tau)\psi(\tau)h(\mathbf{v})$$
$$+ \delta(\mathbf{r})\delta(t),$$

$$P(\mathbf{r}, t) = \int_0^t d\tau \int d\mathbf{v}\nu(\mathbf{r} - \mathbf{v}\tau, t - \tau)\Psi(\tau)h(\mathbf{v}). \quad (2)$$

The first equation describes the events of velocity reorientation [marked by an open circle in Figs. 1(b) and 1(c)], where the density $\nu(\mathbf{r}, t)$ allows us to count the number of particles, $\nu(\mathbf{r}, t)d\mathbf{r}dt$, whose flights ended in the interval $[\mathbf{r}, \mathbf{r} + d\mathbf{r}]$ during the time interval $[t, t + dt]$. The velocity at each reorientation event is chosen from the model-specific velocity distribution $h(\mathbf{v})$ and is statistically independent of the flight time. The second equation relates the events of velocity reorientations to the density of the particles. Here, $\Psi(\tau)$ is the probability to remain in flight for time τ, $\Psi(\tau) = 1 - \int_0^\tau \psi(t')dt'$. The formal solution of the transport equations can be found via a combined Fourier-Laplace transform [18]:

$$P(\mathbf{k}, s) = \frac{\int d\mathbf{v}\Psi(s + i\mathbf{k} \cdot \mathbf{v})h(\mathbf{v})}{1 - \int d\mathbf{v}\psi(s + i\mathbf{k} \cdot \mathbf{v})h(\mathbf{v})}. \quad (3)$$

This is a general answer for a random walk process in arbitrary dimensions with an arbitrary velocity distribution, where $\mathbf{k}$ and s are coordinates in Fourier and Laplace space corresponding to $\mathbf{r}$ and t, respectively (but not for the product model, which is described by *two* independent random walk processes). The microscopic geometry of the process can be captured with $h(\mathbf{v})$. For the XY model we have $h_{XY}(\mathbf{v}) = [\delta(v_y)\delta(|v_x| - v_0) + \delta(v_x)\delta(|v_y| - v_0)]/4$, while for the uniform model it is $h_{uniform}(\mathbf{v}) = \delta(|\mathbf{v}| - v_0)/2\pi v_0$. The technical difficulty is to find the inverse transform of Eq. (3). We therefore employ the asymptotic analysis [1–3] to switch from the Fourier-Laplace representation to the space-time coordinates and analyze model PDFs $P(\mathbf{r}, t)$ in the limit of large $\mathbf{r}$ and t [18].

In the diffusion limit $\gamma > 2$, the mean squared flight length is finite. In the large time limit, the normalized covariance of the flight components in all three models is the identity matrix, and so the cores of their PDFs are governed by the vector-valued central limit theorem [25] and have the universal Gaussian shape $P(\mathbf{r}, t) \simeq \frac{1}{4\pi Dt}e^{-\mathbf{r}^2/4Dt}$, where $D = v_0^2\tau_0/[2(\gamma - 2)]$ (for the product model the velocity has to be rescaled to $v_0/\sqrt{2}$). For the outer parts of the PDFs some bounds can be obtained based

on a theory developed for sums of random variables with slowly decaying regular distributions [26].

The difference between the three walks becomes sharp in the regime of sub-ballistic superdiffusion, $1 < \gamma < 2$. Figure 2 presents the PDFs of the three models obtained by sampling [18] over the corresponding stochastic processes for $t = 10^4 \gg \tau_0 = 1$. These results reveal a striking feature, namely, that the geometry of a random walk is imprinted in its PDF. This is very visual close to the ballistic fronts; however, as we show below, the nonuniversality is already present in the PDF cores.

The PDF of the product model is the product of the PDFs for two identical one-dimensional LWs [3]. In the case of the XY model, the central part of the propagator can be written in Fourier-Laplace space as $P_{XY}(k_x, k_y, s) \simeq (s + \frac{K_\gamma}{2}|k_x|^\gamma + \frac{K_\gamma}{2}|k_y|^\gamma)^{-1}$, where $K_\gamma = \Gamma[2 - \gamma]|\cos(\pi\gamma/2)|\tau_0^{\gamma-1}v_0^\gamma$ [18]. By inverting the Laplace transform, we also arrive at the product of two characteristic functions of one-dimensional Lévy distributions [27,28]: $P_{XY}(k_x, k_y, t) \simeq e^{-tK_\gamma|k_x|^\gamma/2}e^{-tK_\gamma|k_y|^\gamma/2}$. In this case the spreading of the particles along each axis happens twice as slow (note a factor $1/2$ in the exponent) than in the one-dimensional case; each excursion along an axis acts as a trap for the motion along the adjacent axis, thus reducing the characteristic time of the dispersal process by a factor of 2. As a result, the bulk PDF of the XY model is similar to that of the product model after the velocity rescaling, $\tilde{v}_0 = v_0/2^{1/\gamma}$. This explains why on the macroscopic scales the trajectory of the product model, see Fig. 1(e), looks similar to that of the XY model. The difference between the PDFs of these two models appears in the outer parts of the distributions [see Figs. 2(a) and 2(b)]; it cannot be resolved with the asymptotic analysis, which addresses only the central cores of the PDFs. The PDF of the XY model has a crosslike structure with sharp peaks at the ends; see Fig. 3(a). The appearance of these Gothic-like "flying buttresses" [29], capped with "pinnacles," can be

understood by analyzing the process near the ballistic fronts [18].

For the uniform model we obtain $P_{\text{uniform}}(\mathbf{r}, t) \simeq (1/2\pi)\int_0^\infty J_0(kr)e^{-t\tilde{K}_\gamma k^\gamma}k\,dk$, where $\tilde{K}_\gamma = \tau_0^{\gamma-1}v_0^\gamma\sqrt{\pi}\Gamma[2 - \gamma]/\Gamma[1 + \gamma/2]|\Gamma[(1 - \gamma)/2]|$, and $J_0(x)$ is the Bessel function of the first kind (see Ref. [18] for more details). Different from the product and XY models, this is a radially symmetric function that naturally follows from the microscopic isotropy of the walk. Mathematically, the expression above is a generalization of the Lévy distribution to two dimensions [27,30]. However, from the physics point of view, it provides the generalization of the Einstein relation and relates the generalized diffusion constant $\tilde{K}_\gamma$ to the physical parameters of the 2D process, v_0, τ_0, and γ. In Fig. 3(b) we compare the simulation results for the PDF of the uniform model with the analytical expression above.

The regime of ballistic diffusion occurs when the mean flight time diverges, $0 < \gamma < 1$ [20,21]. Long flights dominate the distribution of particles, and this causes the probability concentration at the ballistic fronts. Since the latter are model specific, see Fig. 1, the difference in the microscopic schematization reveals itself in the PDFs even more clearly [18].

Pearson coefficient.—The difference in the model PDFs can by quantified by looking into moments of the corresponding processes. The most common is the MSD, $\langle \mathbf{r}^2(t) \rangle = \int d\mathbf{r}\, r^2 P(\mathbf{r}, t)$. Remarkably, for the XY and uniform models, the MSD is the same as for the 1D Lévy walk with the distribution of flight times given by Eq. (1) [18]. The MSD, therefore, does not differentiate between the XY and uniform random walks (and, if the velocity v_0 is not known *a priori*, the product random walks as well). Next are the fourth-order moments, including the cross-moment $\langle x^2(t)y^2(t) \rangle$. They can be evaluated analytically for all three models [18]. The ratio between the cross-moment and the product of the second moments, $PC(t) = \langle x^2(t)y^2(t) \rangle / \langle x^2(t) \rangle\langle y^2(t) \rangle$, is a scalar characteristic similar to the Pearson coefficient [31,32]. In the asymptotic limit and in the most interesting regime of sub-ballistic
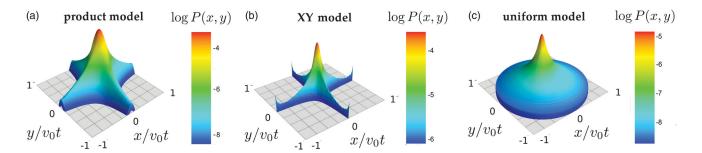

FIG. 2.   Probability density functions of the three models in the superdiffusive regime. The distributions are plotted on a log scale for the time $t/\tau_0 = 10^4$. The PDF for the product model (a) was obtained by multiplying PDFs of two identical one-dimensional LW processes. The PDFs for the XY (b) and uniform (c) models were obtained by sampling over 10^{14} realizations. The parameters are $\gamma = 3/2$, $v_0 = 1$, and $\tau_0 = 1$.
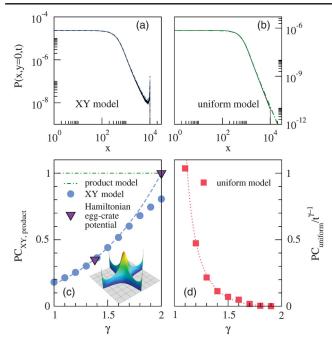
FIG. 3. Statistical features of the models and their Pearson coefficients. (a), (b) The section of the PDF of the *XY* model (a) and uniform model (b) along *x* axis. The results of the statistical sampling for $t = 10^4$ (solid black line) are compared with the analytical results (dashed lines): for the *XY* model it is a product of the one-dimensional Lévy distribution and the function $t^{1/\gamma}(t - x/v)^{-1/\gamma}$ [18]; for the uniform model it is a two-dimensional Lévy distribution. (c),(d) Pearson coefficients for three models. Lines correspond to the asymptotic values Eq. (4), symbols present the results of statistical sampling for the time $t = 10^5$ (error bars are smaller then the symbol size). The *PC*'s for the chaotic Hamiltonian diffusion in an egg-crate potential [23] at time $t = 10^5$, for energy values $E = 4$ (left triangle) and $E = 5.5$ (right triangle), was obtained by sampling over 10^5 independent realizations. The values of the exponent γ, 1.38 and 2, were extracted from the MSD exponent α, $\gamma = 3 - \alpha$. The inset shows the PDF of the process for $t = 10^3$ sampled over 10^8 realizations.

superdiffusion, $1 < \gamma < 2$, this generalized Pearson coefficient equals

$$PC(t) = \begin{cases} 1 & \text{product model} \\ \frac{\gamma\Gamma[4-\gamma]^2}{\Gamma[7-2\gamma]} & XY \text{ model} \\ \frac{(2-\gamma)^2(3-\gamma)^2}{2(4-\gamma)(5-\gamma)(\gamma-1)}\left(\frac{t}{\tau_0}\right)^{\gamma-1} & \text{uniform model.} \end{cases} \quad (4)$$

The *PC* parameter is distinctly different for the three processes: the product model has $PC(t) \equiv 1$, for the *XY* model it is a constant smaller than 1 for any $\gamma \in]1,2]$ and does not depend on v_0 and τ_0, while for the uniform model it diverges in the asymptotic limit as $t^{\gamma-1}$. Figure 3 presents $PC(t = 5 \times 10^5)$ of the *XY* [Fig. 3(c)] and uniform [Fig. 3(d)] models obtained by samplings over 10^{14}

stochastic realizations. We attribute the deviation of the numerical results for the *XY* model from the analytical result Eq. (4) near $\gamma \lesssim 2$ to a slow convergence to the asymptotic limit $PC(t \to \infty)$ [18].

PC can be used to find how close a particular two-dimensional superdiffusive process is to each of the models. The value of γ can be estimated from the MSD exponent α, $\gamma = 3 - \alpha$. To test this idea we investigate a classical two-dimensional chaotic Hamiltonian system [22,23] that exhibits a superdiffusive LW-like dynamics [4,23]. In this system, a particle moves in a dissipationless egg-crate potential and, depending on its total energy, exhibits normal or superdiffusive dispersals [18]. It is reported in Ref. [23] that, for the energy $E = 4$, the dispersal is strongly anomalous, while in Ref. [22] it is stated that the diffusion is normal with $\alpha = 1$, within the energy range $E \in [5,6]$. We sampled the system dynamics for two energy values, $E = 4$ and 5.5. The obtained MSD exponents are 1.62 ± 0.04 and 1 ± 0.02, respectively. We estimated the $PC(t)$ for the time $t = 10^5$ and obtained the values 0.35 and 0.997. The analytical value of the *PC* (4) for the *XY* process with $\gamma = 3 - 1.62 = 1.38$ is 0.355. This *PC* value thus suggests that we are witnessing a superdiffusive *XY* Lévy walk. The numerically sampled PDF of the process [18], see inset in Fig. 3(c), confirms this conjecture.

In contrast to the uniform model, the *PC* parameters for the *XY* and product models are not invariant with respect to rotations of the reference frame, $\{x', y'\} = \{x\cos\phi - y\sin\phi, x\sin\phi + y\cos\phi\}$. While in theory the frame can be aligned with the directions of maximal spread exhibited by an anisotropic particle density at long times, see Figs. 2(a) and 2(b), it might be not so evident in real-life settings. The angular dependence of the *PC* can be explored by rotating the reference frame by an angle $\phi \in [0, \pi/2]$, starting from some initial orientation, and calculating dependence $PC[\phi]$. The result can then be compared to analytical predictions for the asymptotic limit where the three models show different angular dependencies [18]. In addition, the time evolution of $PC[\phi]$ is quantitatively different for the product and *XY* models and thus can be used to discriminate between the two processes. In the product model, the dependence $PC[\phi]$ changes with time qualitatively. For short times it reflects the diagonal ballistic motion of particles and for longer times attains the shape characteristic to the *XY* model [18], an effect that we could already anticipate from inspecting the trajectories in Fig. 1(d). In the *XY* model the positions of minima and maxima of $PC[\phi]$ are time independent.

Conclusion.—We have considered three intuitive models of planar Lévy walks. Our main finding is that the geometry of a walk appears to be imprinted into the asymptotic distributions of walking particles, both in the core of the distribution and in its tails. We also proposed a scalar characteristic that can be used to differentiate between the

types of walks. Further analytical results can be obtained for arbitrary velocity distribution and dimensionality of the problem [33]. For example, it is worthwhile to explore the connections between underlying symmetries of 2D Hamiltonian potentials and the symmetries of the emerging LWs [34].

The existing body of results on two-dimensional super-diffusive phenomena demonstrates that the three models we considered have potential applications. A spreading of cold atoms in a two-dimensional dissipative optical potential [35] is a good candidate for a realization of the product model. Lorentz billiards [36–38] reproduce the XY Lévy walk with exponent $\gamma = 2$. The uniform model is relevant to the problems of foraging, motility of microorganisms, and mobility of humans [3,11,12,39,40]. On the physical side, the uniform model is relevant to a Lévy-like super-diffusive motion of a gold nanocluster on a plane of graphite [41] and a graphene flake placed on a graphene sheet [42]. LWs were also shown, under certain conditions, to be the optimal strategy for searching random sparse targets [13,43]. The performance of searchers using different types of 2D LWs (for example, under specific target arrangements) is a perspective topic [44]. Finally, it would be interesting to explore a nonuniversal behavior of systems driven by different types of multidimensional Lévy noise [45–47].

---

[1] M. F. Shlesinger, J. Klafter, and Y. Wong, J. Stat. Phys. **27**, 499 (1982).

[2] M. F. Shlesinger, B. J. West, and J. Klafter, Phys. Rev. Lett. **58**, 1100 (1987).

[3] V. Zaburdaev, S. Denisov, and J. Klafter, Rev. Mod. Phys. **87**, 483 (2015).

[4] J. Klafter, M. F. Shlesinger, and G. Zumofen, Phys. Today **49**, No. 2, 33 (1996).

[5] Y. Sagi, M. Brook, I. Almog, and N. Davidson, Phys. Rev. Lett. **108**, 093002 (2012).

[6] T. H. Harris, E. J. Banigan, D. A. Christian, C. Konradt, E. D. Tait Wojno, K. Norose, E. H. Wilson, B. John, W. Weninger, A. D. Luster, A. J. Liu, and C. A. Hunter, Nature (London) **486**, 545 (2012).

[7] C. Ariel, A. Rabani, S. Benisty, J. D. Partridge, R. M. Harshey, and A. Be'er, Nat. Commun. **6**, 8396 (2015).

[8] D. A. Raichlen, B. M. Wood, A. D. Gordon, A. Z. P. Mabulla, F. W. Marlowe, and H. Pontzer, Proc. Natl. Acad. Sci. U.S.A. **111**, 728 (2014).

[9] G. M. Fricke, F. Asperti-Boursin, J. Hecker, J. Cannon, and M. Moses, Adv. Artif. Life ECAL **12**, 1009 (2013).

[10] J. Beal, ACM Trans. Auton. Adapt. Syst. **10**, 1 (2015).

[11] V. Méndez, D. Campos, and F. Bartumeus, *Stochastic Foundations in Movementecology* (Springer, Berlin, 2014).

[12] G. Viswanathan, M. da Luz, E. Raposo, and H. Stanley, *The Physics of Foraging: An Introduction to Random Searches and Biological Encounters* (Cambridge University Press, Cambridge, England, 2011).

[13] O. Bénichou, C. Loverdo, M. Moreau, and R. Voituriez, Rev. Mod. Phys. **83**, 81 (2011).

[14] B. Gnedenko and A. Kolmogorov, *Limit Distributions for Sums of Independent Random Variables* (Addison-Wesley, Reading, MA, 1954).

[15] F. Spitzer, *Principles of Random Walks* (Springer, New York, 1976).

[16] J. Klafter and I. M. Sokolov, *First Steps in Random Walks* (Oxford University Press, New York, 2011).

[17] K. Pearson, Nature (London) **72**, 294 (1905).

[18] See Supplemental Material at http://link.aps.org/supplemental/10.1103/PhysRevLett.117.270601, which includes Refs. [19–24], for additional figures and details of calculations.

[19] A. Erdélyi, *Tables of Integral Transforms* (McGraw-Hill, New York, 1954), Vol. 1.

[20] D. Froemberg, M. Schmiedeberg, E. Barkai, and V. Zaburdaev, Phys. Rev. E **91**, 022131 (2015).

[21] M. Magdziarz and T. Zorawik, Phys. Rev. E **94**, 022130 (2016).

[22] T. Geisel, A. Zacherl, and G. Radons, Phys. Rev. Lett. **59**, 2503 (1987).

[23] J. Klafter and G. Zumofen, Phys. Rev. E **49**, 4873 (1994).

[24] J. Laskar and P. Robutel, Celest. Mech. Dyn. Astron. **80**, 39 (2001).

[25] A. W. Van der Vaart, *Asymptotic Statistics* (Cambridge University Press, Cambridge, England, 1998).

[26] A. A. Borovkov and K. A. Borovkov, *Asymptotic Analysis of Random Walks: Heavy-Tailed Distributions* (Cambridge University Press, Cambridge, England, 2008).

[27] V. Uchaikin and V. Zolotarev, *Chance and Stability: Stable Distributions and Their Applications, Modern Probability and Statistics* (De Gruyter, Berlin, 1999).

[28] A. A. Dubkov, B. Spagnolo, and V. V. Uchaikin, Int. J. Bifurcation Chaos Appl. Sci. Eng. **18**, 2649 (2008).

[29] J. Heyman, *The Stone Skeleton* (Cambridge University Press, Cambridge, England, 1997).

[30] J. P. Taylor-King, R. Klages, S. Fedotov, and R. A. Van Gorder, Phys. Rev. E **94**, 012104 (2016).

[31] K. Pearson, Proc. R. Soc. London **58**, 240 (1895).

[32] J. F. Kenney and E. S. Keeping, *Mathematics of Statistics* (Van Nostrand, Prindeton, NJ, 1951), Part 2.

[33] I. Fouxon, S. Denisov, V. Zaburdaev, and E. Barkai (unpublished).

[34] G. M. Zaslavsky, M. Edelman, and B. A. Niyazov, Chaos **7**, 159 (1997).

[35] S. Marksteiner, K. Ellinger, and P. Zoller, Phys. Rev. A **53**, 3409 (1996).

[36] Ya. G. Sinai, Russ. Math. Surv. **25**, 137 (1970).

[37] J.-P. Bouchaud and A. Georges, Phys. Rep. **195**, 127 (1990).

[38] G. Cristadoro, T. Gilbert, M. Lenci, and D. P. Sanders, Phys. Rev. E **90**, 050102 (2014).

[39] N. E. Humphries, H. Weimerskirch, and D. W. Sims, Methods Ecol. Evol. **4**, 930 (2013).

[40] G. C. Hays, T. Bastian, T. K. Doyle, S. Fossette, A. C. Gleiss, M. B. Gravenor, V. J. Hobson, N. E. Humphries, M. K. S. Lilley, N. G. Pade, and D. W. Sims, Proc. R. Soc. B **279**, 465 (2012).

[41] W. D. Luedtke and U. Landman, Phys. Rev. Lett. **82,** 3835 (1999).

[42] I. V. Lebedeva, A. A. Knizhnik, A. M. Popov, O. V. Ershova, Y. E. Lozovik, and B. V. Potapkin, Phys. Rev. B **82,** 155460 (2010).

[43] G. M. Viswanathan, S. V. Buldyrev, S. Havlin, M. G. E. da Luz, E. P. Raposo, and H. E. Stanley, Nature (London) **401,** 911 (1999).

[44] M. Chupeau, O. Bénichou, and R. Voituriez, Nat. Phys. **11,** 844 (2015).

[45] A. La Cognata, D. Valenti, A. A. Dubkov, and B. Spagnolo, Phys. Rev. E **82,** 011121 (2010).

[46] C. Guarcello, D. Valenti, A. Carollo, and B. Spagnolo, J. Stat. Mech. (2016) 054012.

[47] D. Valenti, C. Guarcello, and B. Spagnolo, Phys. Rev. B **89,** 214510 (2014).